PROCEEDINGS A

rspa.royalsocietypublishing.org

Research

Article submitted to journal

Subject Areas:
mechanical engineering, differential equations

Keywords:
Hopf bifurcation, feedback control, limit cycle, stabilization

Author for correspondence:
K.H. Lee
e-mail: jz18526@bristol.ac.uk

THE ROYAL SOCIETY
PUBLISHING

Stabilizing limit cycle oscillation using control based continuation near Hopf bifurcation

K.H. Lee[1], D.A.W. Barton[1] and L. Renson[1]

[1]Department of Engineering Mathematics, University of Bristol

CBC scheme for Hopf bifrucation and it's application on system identification is studied. We consider dynamical system without control has codimension-1 Hopf bifurcation. Then, the dynamical system with proportional derivative feedback control applied to this system has codimension-3 Hopf bifurcation where two control gains are added as an additional unfolding parameter. Bifurcation of the dynamical system that has Hopf bifurcation can be simplified when center manifold theory and normal form theory is applied. If we assume weakly nonlinear transformation between the original coordinates and the normal form coordinates, the limit cycle of the uncontrolled system can be expressed as a single harmonic oscillator in original coordinates, and it can be shown that system with control can be simplified to forced Hopf bifurcation with single harmonic forcing. Stabilizability of the controller can be derived from the stability of the noninvasive periodic solution, which is one of phase-locked periodic solution of the forced Hopf bifurcation. Finding this noninvasive periodic solution can be simplified if the only phase-locked periodic solutions are searched through experiment; therefore, we introduce a scheme to lock the phase between the control target and the response and show that finding noninvasive control target is equivalent to solving zero problems of one-dimensional function in a certain type of dynamical system. Developed CBC scheme is applied to flutter rig that has codimension-1 subcritical Hopf bifurcation. We show flutter frequency and flutter speed can be estimated from the CBC results and can be applied to verify the identified linearized dynamical model. Finally, we show that CBC results can be applied to identify the nonlinear part of the dynamical system if the LCO is parametrized with unknown parameters by computed normal form.

1. Introduction

Feedback control can be used as a tool to verify the dynamical

model or also as an identifying tool when it is noninvasive. Time delyaed feedback (TBD) [1, 2] is popular feedback control scheme that feeds a signal $x(t)-x(t-T)$ back where $x(t)$ is output of the experiment and T is period of the periodic orbit subject to be stabilized. Control-based continuation (CBC) resembles the approach of delayed feedback by replacing delay signal $x(t-T)$ to time-periodic signal $x^*(t)$ which also reduces difficulties dealing with delayed signals such as memory problems and measurement noise. CBC scheme is generally solving fixed point problem experimentally, which is based on finding noninvasive control target that stabilizes unstable periodic orbit of the uncontrolled system.

CBC was initially proposed by Sieber and Krauskopf [3] and applied to wide range of mechanical system experiments, parametrically excited pendlum [4], impact oscillators [5, 6], nonlinear energy harvester [7, 8] , and cantilever beam with a nonlinear mechanism at its free tip [9]. Also, CBC has been proved to produce critical information about nonlinear dynamical systems such as nonlinear normal modes [10, 11] and floquet multipliers [12] and harmonically coupled modes [9].

Limit cycle oscillation (LCO) of self-excited system is also an essential subject for researchers. Hopf bifurcation would be the typical example of self-excited system produced by loss of stability of equilibrium with parameter variation and birth of a family of LCO near the bifurcation point. LCOs are either stable(supercritical Hopf bifurcation) or unstable(subcritical Hopf bifurcation) close to Hopf bifurcation, and it can be analyzed analytically by simplifying the dynamical system [13, 14] or numerical continuation methods [15, 16]. Subcritical Hopf bifurcation is problematic in many engineering applications such as flutter of aircraft wings and shimmying in wheels. Therefore, stabilizing unstable LCOs of subcritical Hopf bifurcation using feedback control is a critical subject for experimentalists. Stabilizability of the feedback controller for subcritical Hopf bifurcation problems using TBD was studied theoretically [17, 18]. However, there are several difficulties in real experiments using feedback control methods. For TBD, LCO cannot be stabilized if the period of the LCO is unknown. For CBC, input-output map is more complicated compared to typical forced dynamical systems since the feedback-controlled system is forced Hopf bifurcation. Let us say time-periodic control target $x^*(t)$ and time-periodic response $x(t)$ is discretized by Φ which is a projection of periodic orbit to first three fourier modes as

$$\Phi(x^*(t))=[\hat{A}_0,\hat{A}_1,\hat{B}_1],\ \Phi(x(t))=[A_0,A_1,B_1], \tag{1.1}$$

then, zero problem can be defined at each fourier modes and solved by newton like methods for typical CBC applications that have a bijective input-output map. However, the response of forced Hopf bifurcation has an infinite set of steady-state solutions that has phase difference when a single harmonic force is applied to the system [19]. An infinite set of $[A_0,A_1,B_1]$ can be found with phase difference for Hopf bifurcation for every set of $[\hat{A}_0,\hat{A}_1,\hat{B}_1]$; therefore, zero problem cannot be defined for Hopf bifurcation problem if typical CBC scheme is used. The aim of this paper is a theoretical explanation of stabilizing feedback control of Hopf bifurcation using CBC and developing an effective scheme that is applicable to experimental bifurcation analysis.

Rest of the paper is formulated as follows. In the second section, the general idea of CBC scheme is presented. In the third section, theory to simplify the dynamics of Hopf bifurcation is introduced, and we show that CBC applied to Hopf bifurcation is equivalent to forced Hopf bifurcation with single harmonic forcing if weakly nonlinear transformation is assumed. Stabilizability of the controller is discussed and CBC scheme to lock the phase between the control target and the output response is proposed. Effective experimental scheme to find the stabilizability of the controller and to find noninvasive periodic solution is developed for a dynamical system that has small frequency variance while multiple measurements of phase-locked periodic orbits are taken with fixed amplitude of control target. In the fourth section, the proposed CBC scheme is applied experimentally to flutter rig that has subcritical Hopf bifurcation. Application of CBC results in linear system verification, and nonlinear parameter identification is presented in the fifth section.

2. Control based continuation (CBC)

Let us say proportional derivative control is applied to some dynamical system and control force $\Gamma(t)$ is

$$\Gamma(t) = K_p(x^*(t) - x(t)) + K_d(\dot{x}^*(t) - \dot{x}(t)), \tag{2.1}$$

where $x(t)$ is a scalar output of the system and $x^*(t)$ is a scalar control target. If K_p,K_d are selected appropriately to stabilize the unstable periodic orbit of uncontrolled system, zero problem defined by input and output $x^*(t) - x(t) = 0$ can be solved by projecting $x^*(t)$ and $x(t)$ to first $2q+1$ fourier modes. This projection gives discretized fixed point problem with $2q+1$ equations. Fixed point problem of CBC can be embedded to pseudo arclength continuation by including additional zero problem and path-following of the family of periodic orbit can be similarly established with numerical continuation methods. We use proportional derivative control in this research. However, CBC scheme is not restricted to only proportional derivative control.

Stabilizing unstable LCO with CBC is not simple because of the complexity of the input-output map of forced Hopf bifurcation. Zero problem to be solved in the experiment cannot be defined if we use a typical CBC scheme that discretizes periodic orbit with first $2q+1$ fourier coefficients. We will discuss the input-output map of CBC for Hopf bifurcation and a scheme to define a zero problem from the input-output map in the next section.

3. Stablizing control near the Hopf bifurcation

Simplifying the dynamical system using normal form is the most popular way to study the bifurcation problem analytically. There are numerous tools to derive normal form, for example, center manifold reduction, Liapunov-Shmidt reduction and method of multiple scales. In this research, we focus on studying controlled and uncontrolled dynamics near the Hopf bifurcation via center manifold reduction, near-identity transformation, time, and unfolding parameter rescaling to discuss the stabilizability of the controller.

(a) Simplest normal form of Hopf bifurcation

Let us consider an autonomous nonlinear parameter-dependent dynamical system that has generic Hopf bifurcation at $\lambda = 0$,

$$\dot{\mathbf{z}} = \mathbf{F}(\mathbf{z}, \lambda), \tag{3.1}$$

where $\mathbf{z} \in \mathbb{R}^n$ is state variable and $\lambda \in \mathbb{R}^m$ is a control parameter. We assume $\mathbf{F}(0) = 0$ and $\mathbf{F}$ is a C^r function with $r > 3$. (3.1) can be transformed to Jordan normal form as a partioned system at $\lambda = 0$ by transforming the linearization of $\mathbf{F}$ to Jordan normal form as

$$\begin{aligned} \dot{\mathbf{x}} &= \mathbf{J}_c\mathbf{x} + \mathbf{f}(\mathbf{x}, \mathbf{y}, \lambda) \\ \dot{\mathbf{y}} &= \mathbf{J}_s\mathbf{y} + \mathbf{g}(\mathbf{x}, \mathbf{y}, \lambda) \end{aligned} \tag{3.2}$$

where $\mathbf{x} = [x; \bar{x}] \in \mathbb{C}^2$ is center subspace with associated Jordan matrix $\mathbf{J}_c$ having diagonal term $\pm$i and $\mathbf{y} \in \mathbb{C}^{n-2}$ is stable subspace with it's associated Jordan matrix $\mathbf{J}_s$ of Jacobian of $\mathbf{F}(\mathbf{z})$ at $\mathbf{z} = 0$. $\mathbf{f}$ and $\mathbf{g}$ are C^r functions with $\mathbf{f}(0,0) = 0$, $D\mathbf{f}(0,0) = 0$ and $\mathbf{g}(0,0) = 0$, $D\mathbf{g}(0,0) = 0$. Centermanifold exists for dynamical system (3.2) for small $\|\mathbf{x}\|$ which is invariant under the action of dynamical system [20]. Note that eigenvalues corresponding to center subspace is assumed $\pm$i for simplicity. To reduce the order of dynamics of Hopf bifurcation, we include $\dot{\lambda} = 0$ to (3.2) and analyze the family of center manifolds, locally represented by small $\|\lambda\|$ [21]. power series of centermanifold $\mathbf{H}(\mathbf{x}, \lambda)$ can be computed recursively by solving

$$D\mathbf{H}(\hat{\mathbf{x}})(\hat{\mathbf{J}}_c\hat{\mathbf{x}} + \mathbf{f}(\hat{\mathbf{x}}, \mathbf{H}(\hat{\mathbf{x}}))) = \mathbf{J}_s\mathbf{H}(\hat{\mathbf{x}}) - \mathbf{g}(\hat{\mathbf{x}}, \mathbf{H}(\hat{\mathbf{x}})) \tag{3.3}$$

at each order of power series, where $\hat{\mathbf{x}} = [\lambda; \mathbf{x}]$ and $\hat{\mathbf{J}}_c$ is the extended Jordan matrix which zero eigenvalue is added to $\mathbf{J}_c$ [22]. Then, we can compute the reduced dynamics on the centermanifold as a power series which will have a form as

$$\begin{aligned}\dot{x} &= \mathrm{i}x + \sum_k f_k(x,\bar{x},\lambda)\\ \text{,where } f_k &= \sum_{j+l+m=k} (\mathbf{a}_{1jlm} + \mathrm{i}\mathbf{a}_{2jlm}) x^j \bar{x}^l \lambda^m.\end{aligned} \tag{3.4}$$

Note that in (3.4), $\lambda = [\lambda_1;\lambda_2;\ldots;\lambda_m]$ and λ^m denotes $\lambda_1^{m_1}\lambda_2^{m_2}\cdots\lambda_m^{m_m}$ satisfying $\sum_i m_i = m$ with $\mathbf{a}_{1jlm} = [a_{1jlm_1};a_{1jlm_2};\ldots;a_{1jlm_m}]$.

Recently, researchers have worked extensively to develop an efficient simplest normal form of Hopf bifurcation using computer algebra [23, 24]. Simplest normal form(SNF), simplest means that the number of terms retained at each order of is minimized, is one of the most effective ways to derive the normal form from the nonlinear differential equation defined on center manifold. Unlike the dynamical system without perturbation parameters, SNF cannot be computed using only near identity transformation. P.Yu[13] proved time and parameter rescaling is essential additional to near identity transformation and developed a recursive formula to compute SNF up to k-th order; however, we limit our attention up to third order. SNF can be expressed as

$$\begin{aligned}\frac{du}{d\tau} &= (\alpha_1 + \mathrm{i}\beta_1)\nu u + (\alpha_2 + \mathrm{i}\beta_2)u^2\bar{u} + \sum_k g_k(u,\bar{u}),\\ \text{where } g_k(u,\bar{u}) &= (b_{1k} + \mathrm{i}b_{2k})u^{\frac{k+1}{2}}\bar{u}^{\frac{k-1}{2}}, \text{ for odd integer } k.\end{aligned} \tag{3.5}$$

Here, $\mathbf{u} = [u,\bar{u}]$ and equation of complex conjugate variable $\bar{u}$ is neglected. u,τ and ν are transformed from x,t and λ by following near identity transformation $x = h(u,\bar{u},\nu)) = u + \sum_k h_k(u,\bar{u},\nu)$, time rescailing $t = T(u,\bar{u},\nu,\tau)$ and parameter rescailing $\lambda = p(\nu)$,

$$\begin{aligned}h_k &= \sum_{j+l+m=k} (c_{ijkm} + \mathrm{i}c_{2jlm}u^j\bar{u}^l\nu^m),\\ t &= \left(1 + \sum_{k=1}\sum_{j+m=k} t_{jm}[(u+\bar{u})]^j\nu^m\right)\tau,\\ \lambda &= \nu + \sum_{j=2} p_j\nu^j.\end{aligned} \tag{3.6}$$

Coefficients of (3.6) can be computed recursively by solving the following equations [13]:

$$\begin{aligned}g_2(\mathbf{u},\nu) &= f_2(\mathbf{x},\lambda) + [h_2(\mathbf{u},\nu),l(\mathbf{u})] + (T_1(\mathbf{u},\nu)l(\mathbf{u}) - Dh_1(\mathbf{u},\nu)L_2(\mathbf{u},\nu)),\\ g_3(\mathbf{u},\nu) &= f_3(\mathbf{x},\lambda) + [h_3(\mathbf{u},\nu),l] + (Df_2(\mathbf{x},\lambda)\tilde{h}_2(\mathbf{u},\nu) - Dh_2(\mathbf{u},\nu)g_2(\mathbf{u},\nu))\\ &\quad + T_1(\mathbf{u},\nu)(f_2(\mathbf{x},\lambda) + J_c h_2(\mathbf{u},\nu)] + (T_2(\mathbf{u},\nu)l(\mathbf{u}) - Dh_2(\mathbf{u},\nu)L_2(\mathbf{u},\nu)),\end{aligned} \tag{3.7}$$

where $l(\mathbf{u}) = \mathbf{J}_c\mathbf{u}$, $\tilde{h}_2 = [h_2;p_2]$, and $\left[h_k,l\right]$ is Lie bracket defined as

$$\left[h_k,l\right] = Dl\cdot h_k - Dh_k\cdot l. \tag{3.8}$$

Eliminating noncritical terms by applying (3.6) transformation to (3.7) and balancing every coefficient of power series, SNF of Hopf bifurcation is derived as

$$\frac{du}{d\tau} = \mathrm{i}u + \mathbf{a}_{1101}\nu u + (a_{1210} - a_{1200}a_{2110} - a_{2200}a_{1110})u^2\bar{u} + \mathrm{i}\sum_{m=1} b_{2(2m+1)}u^{m+1}u^m. \tag{3.9}$$

This can be expressed in a more simpler form by transforming to polar coordinates,

$$\begin{aligned}\frac{dR}{d\tau} &= \mathbf{a}_{1101}\nu R + (a_{1210} - a_{1200}a_{2110} - a_{2200}a_{1110})R^3\\ \frac{d\theta}{d\tau} &= 1 + b_{23}R^2.\end{aligned} \tag{3.10}$$

The stability of limit cycle can be analyzed from (3.10); for instance, Hopf bifurcation is subcritical if $a_{1210} - a_{1200}a_{2110} - a_{2200}a_{1110} < 0$ for codimension-1 case.

(b) Stabilizability of controller

We will consider linear proportional derivative control acting on a single coordinate vector which will be the most simple case to setup a nonlinear dynamic experiment in various applications. We will consider the autonomous dynamical system that has codimension-1 generic subcritical Hopf bifurcation at $\mu = 0$,

$$\dot{\mathbf{z}} = \mathbf{G}(\mathbf{z}, \mu). \tag{3.11}$$

where, $\mu \in \mathbb{R}$ is an unfolding parameter, and we assume $z_{j+1} = \dot{z}_j$ for all odd j. To stabilize the unstable periodic orbit near the Hopf bifurcation point, we add a proportional derivative feed-back control to (3.11). Let us assume that the control force is applied in the direction of the one principle coordinates to (3.11),

$$\dot{\mathbf{z}} = \mathbf{G}(\mathbf{z}, \mu) + \mathbf{e}_{j+1}(K_p(z^*(t) - z_j) + K_d(\dot{z}^*(t) - z_{j+1})), \tag{3.12}$$

where, $\mu \in \mathbb{R}$ is an control parameter of uncontroled system, $\mathbf{e}_{j+1}$ is $j+1$ th standard basis, K_p is the proportional control gain, K_d is the derivative control gain, z_j, z_{j+1} are monitored signal for the control, and $z^*(t)$ is the time periodic control target. We can rewrite (3.12) in autonomous form by droping off the time periodic forcing $e_{j+1}(K_p(z^*(t)) + K_d(\dot{z}^*(t)))$ as

$$\dot{\mathbf{z}} = \mathbf{G}(\mathbf{z}, \mu) - \mathbf{e}_{j+1}(K_p z_j + K_d z_{j+1}). \tag{3.13}$$

We can rewrite (3.13) in the form of (3.1) by

$$\begin{aligned} F(\mathbf{z}) =& \mathbf{G}(\mathbf{z}, \mu) - \mathbf{e}_{j+1}(K_p z_j + K_d z_{j+1}) \\ \lambda =& [\mu, K_p, K_d]^T. \end{aligned} \tag{3.14}$$

(3.14) has codimension-3 Hopf bifurcation at $\lambda = 0$. As explained in Subsection (a), we can derive the reduced dynamics on center manifold of (3.14) and compute SNF using nonlinear transformation between origianl coordinates $[x, \bar{x}]^T$ and normal form coordinates $[u, \bar{u}]^T$ and rescailing time and unfolding parameters. We will study the stabilizability of unstable limit cycle of the uncontroled system at $\lambda = \lambda_1 = [\mu, 0, 0]^T$ by using CBC. Limit cycle($[u_1(\tau), \bar{u}_1(\tau)]^T$) is a nonzero fixed point of (3.10) and expressed in normal form coordinates $[u, \bar{u}]^T$ as

$$\begin{aligned} u_1(\tau) =& R_1 e^{\mathrm{i}\omega_1 \tau}, \\ \bar{u}_1(\tau) =& R_1 e^{-\mathrm{i}\omega_1 \tau}, \end{aligned} \tag{3.15}$$

where R_1 is the amplitude and ω_1 is frequency of the limit cycle in rescailed time. If we define homeomorphism($\Psi_1 : \mathbb{C} \times \mathbb{C} \to \mathbb{C} \times \mathbb{C}$) between the original coordinates $[x, \bar{x}]^T$ and normal form coordinates $[u, \bar{u}]^T$ at $\lambda = \lambda_1$ as

$$[x, \bar{x}]^T = \Psi_1(u, \bar{u}) = [h(u, \bar{u}, \nu_1), \bar{h}(u, \bar{u}, \nu_1)]^T, \tag{3.16}$$

where $\nu_1 = p^{-1}(\lambda_1)$ is unfolding parameter reparametrization in the coordinates of the normal form. Limit cycle (3.15) in original coordinates $x^*(t)$ can be computed from

$$[x^*(t), \bar{x^*}(t)]^T = \Psi_1(R_1 e^{\mathrm{i}\omega_1 \tau}, R_1 e^{-\mathrm{i}\omega_1 \tau}). \tag{3.17}$$

Definition 3.1. ***Noninvasive periodic solution*** *is a periodic solution of dynamical system where control force is zero.*

Lemma 3.1. *$z(t) = \Sigma^{-1}x^*(t)\Sigma$ is a noninvasive periodic solution for (3.12) if and only if $z^*(t) = p_c x^*(t)$. where $\Sigma$is a coordinate transformation matrix to Jordan normal form at $\lambda = 0$ and $p_c =< \xi_c, \mathbf{e}_j >$ is a scalar projection of center space modal vector ξ_c to $\mathbf{e}_j$.*

Proof. If $z^*(t) = p_c x^*(t)$, by inserting $z(t) = \Sigma^{-1}x^*(t)\Sigma$ to (3.12), we have $\mathbf{G}(\mathbf{z}, \mu) = 0$ and $z^*(t) - z_j = 0$. For the only if part, lets assume $z(t) = \Sigma^{-1}x^*(t)\Sigma$ is a noninvasive periodic solution. Then, $z^*(t) = p_c x^*(t)$ since the solution is noninvasive. □

Let $\lambda_2 = [\mu, K_p, K_d]$ and we will analyze the stability of the noninvasive periodic solution $z(t) = \Sigma^{-1}x^*(t)\Sigma$ with control target $z^*(t) = p_c x^*(t)$ at $\lambda = \lambda_2$. To simplify the problem, we make an assumption on the coefficeints of $h(\mathbf{u}, \nu)$.

Assumption 3.1. *For $\lambda = \lambda_1$ and $\lambda = \lambda_2$, we assume coefficients of near identity transformation in (3.6) c_{1ijlm}, c_{2ijlm} is very samll for $i + j \geq 2$.*

If we use Assumption 3.1, periodic solutions in the normal form will be transformed into a single harmonic oscillator in the original coordinates. Therefore, using the result of Lemma 3.1 we can write limit cycle in original coordinates $x^*(t)$ and control target $z^*(t)$ as a single harmonic oscillator,

$$\begin{aligned} x^*(t) =& R_0 e^{\mathrm{i}\omega_0 t}, \\ z^*(t) =& p_c x^*(t) = p_c R_0 e^{\mathrm{i}\omega_0 t}. \end{aligned} \tag{3.18}$$

Note that ω_1 in (3.17) is rescaled frequency of LCO from ω_0 at $\lambda = \lambda_0$. By putting (3.18) to (3.12) nonautonomous term of (3.12) is a single harmonic oscillator, and our problem to be solved is Hopf bifurcation with single harmonic forcing. The normal form of forced Hopf bifurcation for small amplitude bounded solution is equivalent to adding force in the direction of the centerspace to the autonomous Hopf normal form [25, 26]. Therefore, if we define ε as an amplitude of periodic forcing which is rescaled in the normal form coordinates, normal form with single harmonic forcing at $\lambda = \lambda_2$ can be derived as

$$\frac{du}{d\tau} = (\alpha_1 + \mathrm{i}\beta_1)u + (\alpha_2 + \mathrm{i}\beta_2)u^2\bar{u} + \varepsilon e^{\mathrm{i}\omega_2\tau}, \tag{3.19}$$

where coefficients α_1, α_2, β_1, and β_2 can be computed from (3.9) using the coefficients of reduced dynamics at the centermanifold and ω_2 is rescaled frequency of external forcing in the normal form coordinates. Stabilizability of the control can be anlyzed by the stability of the periodic solution of (3.19) $u = u_2(\tau)$, where $u_2(\tau)$ is transfromed from $x^*(t)$ by

$$[u_2(\tau), \bar{u}_2(\tau)]^T = \Psi_2^{-1}(R_0 e^{\mathrm{i}\omega_0 t}, R_0 e^{-\mathrm{i}\omega_0 t}), \tag{3.20}$$

where homeomorphism($\Psi_2 : \mathbb{C} \times \mathbb{C} \to \mathbb{C} \times \mathbb{C}$) is defined at $\lambda = \lambda_2$ as

$$[x, \bar{x}]^T = \Psi_2(u, \bar{u}) = [h(u, \bar{u}, \nu_2), \bar{h}(u, \bar{u}, \nu_2)]^T. \tag{3.21}$$

Note that ν_2 can be computed as $\nu_2 = p(\lambda_2)$. Under Assumption 3.1, $u_2(\tau)$ is a single harmonic oscillator which is phase locked with $\varepsilon e^{\mathrm{i}\omega_2\tau}$.

Lemma 3.2. *Noninvasive periodic solution $u_2(\tau)$ is stable if the amplitude of the solution R_2 satisfies*

$$3(\alpha_2^2 + \beta_2^2)R_2^3 + 4(\alpha_1 + \beta_2(\beta_1 - \omega_2))R_2 + (\alpha_1^2 + (\beta_1 - \omega_2)^2) < 0. \tag{3.22}$$

Proof. If we look (3.19) in the rotating coordinates defined by

$$v = ue^{i\omega_2\tau}, \tag{3.23}$$

The dynamical system becomes autonomous,

$$\dot{v} = (\alpha_1 + i(\beta_1 - \omega_2))v + (\alpha_2 + i\beta_2)v^2\bar{v} + \varepsilon. \tag{3.24}$$

v satisfying $\dot{v} = 0$ is a phase locked periodic solution with the forcing of (3.19). We obtain algebraic equation by setting $\dot{v} = 0$,

$$((\alpha_1 + \alpha_2 R^2) + i((\beta_1 - \omega_2) + \beta_2 R^2)))v = -\varepsilon. \tag{3.25}$$

We can derive $P(R)$, where the zeros of $P(R)$ is phase locked periodic solutions of (3.19), by taking norm square of both side of (3.25)

$$P(R) = (\alpha_2^2 + \beta_2^2)R^6 + 2(\alpha_1 + \beta_2(\beta_1 - \omega_2))R^4 + (\alpha_1^2 + (\beta_1 + \omega_2)^2)R^2 - \varepsilon^2 = 0. \tag{3.26}$$

Since the noninvasive periodic solution is phase locked solution of (3.19) at $R = R_2$. Dividing $P_R(R_2)$ by $2R_2^2$, we arrive to the stability condition of the noninvasive periodic solution. □

The controller is able to stabilize the unstable LCO of the uncontrolled system if the noninvasive periodic solution is stable. For CBC experiments, finding noninvasive control target remains as a problem even if the controller is stabilizable. This will be discussed in the next subsection.

(c) Scheme for finding noninvasive periodic solution

In many nonlinear dynamic experiments, information about the dynamical system is not given; therefore, noninvasive periodic solution and stabilizability of the control cannot be determined from the equation as in Section (a). We will discuss effective scheme to find noninvasive periodic solutions near the Hopf bifurcation point in this subsection. The response of system with control (3.22) is very complicated. There are multiple periodic solutions at given forcing frequency ω_2 and forcing amplitude ε, see [27, 28] for detailed bifurcation diagram of this type of oscillator. It is clear that noninvasive periodic solution is in phase with the forcing frequency; however, solutions of (3.22) are not necessarily to be in phase with forcing frequency. For example, if we set rotating coordinates of (3.23) $v = ue^{i(\omega_2\tau - \theta)}$, where θ is an arbitrary phase shift, we can rewrite (3.19) as

$$\frac{du}{d\tau} = (\alpha_1 + i\beta_1)u + (\alpha_2 + i\beta_2)u^2\bar{u} + \varepsilon e^{i\theta}. \tag{3.27}$$

A stationary solution of (3.27) with arbitrary phase shift θ is also a periodic response of the controlled system. This phase shift of the response and control target depends on initial condition, which is uncontrollable. Therefore, it makes the problem much simpler if we can force the response to be in phase with a control target to determine the noninvasive periodic solution.

We use a real-time controller to achieve phase locking between target coefficients $z^*(t)$ with the response in (3.12). This is equivalent to phase-locking between force and response in (3.22), which was first proposed in [29]. We assume that monitored signals z_j, z_{j+1} can be expressed as an analytic signal,

$$\begin{aligned} z_j(t) &= A(t)\cos\phi, \\ z_{j+1}(t) &= -\dot{\phi}A(t)\sin\phi \end{aligned} \tag{3.28}$$

where $A(t)$ is the instantaneous amplitude, ϕ is the instantaneous phase of the response, $\dot{\phi}$ is the frequency of the response which is constant if the system is at the steady-state. To lock the phase, we can set the target coefficient as

$$z^*(t) = \hat{A}\cos\phi = \hat{A}\cos\left(\tan^{-1}\left(\frac{-z_{j+1}(t)}{\dot{\phi} z_j(t)}\right)\right), \tag{3.29}$$

where $\hat{A}$ is the amplitude of the control target, if we update $\dot{\phi}$ every fixed time interval from the measurement and wait until the system reaches the steady-state, final steady-state solution is one of the stable phase-locked solution of (3.19). Note that $\varepsilon = \varepsilon(\hat{A})$ can be rescaled from $\hat{A}$ in normal form coordinates. We cannot adjust the frequency of the target if we use this scheme; however, we make the finding noninvasive periodic solution problem solvable on a certain type of dynamical systems. First, we define the family of stable phase-locked periodic solutions by solutions of (3.26) with $\hat{A} \in V$ on normal form coordinates, where $V \subset \mathbb{R}$ is some set containing small amplitude of control targets. Family of phase-locked periodic solutions with fixed $\varepsilon(\hat{A})$ lies on two-dimensional space (R, ω) consisting amplitude and frequency, which is a solution of (3.26). We can define the family of stable phase-locked solution as

Definition 3.2. *Family of stable phase locked periodic solutions on* $\hat{A} \in V$

$$\begin{aligned} S_{\hat{A}} &= \{(R,\omega) \in \mathbb{R}^2 | P(R) = 0; P_R(R) < 0; \varepsilon = \varepsilon(\hat{A})\}, \\ S_V &= \bigcup_{\hat{A}\in V} S_{\hat{A}}. \end{aligned} \tag{3.30}$$

Note that experimentally measured phase-locked solution with fixed $\hat{A}$ is an element of $S_{\hat{A}}$, and we assume for $(R, \omega) \in S_V$, R is a smooth function of ω and $\varepsilon(\hat{A})$. Based on our experimental observations, we define a certain type of S_V that has small frequency variance while taking multiple sets of measurements with $\hat{A} \in V$, and we define this type of S_V as

Definition 3.3. *S_V is constant frequency family of stable phase locked periodic orbit if* $\varpi = \sup\{(\|\omega_a - \omega_b\| | \omega_a \in W_{\hat{A}}$ *and* $\omega_b \in W_{\hat{A}}\}$ *is sufficiently small for all* $\hat{A} \in V$*, where*

$$\begin{aligned} W_{\hat{A}} &= \{\Omega(R,\omega) | (R,\omega) \in S_{\hat{A}}\}, \\ \Omega(R,\omega) &:= \omega. \end{aligned} \tag{3.31}$$

Golubitsky [19] showed that maximum of $R(\omega)$ is bounded at fixed forcing amplitude; therefore, $R(\omega)$ is bounded in a very small interval at every fixed $\hat{A} \in V$ for constant frequency S_V. We assume that amplitude of phase-locked periodic solution depends only on forcing amplitude, i.e. $R = R(\varepsilon(\hat{A}))$, for constant frequency S_V. Now zero problem can be defined with simple input $\hat{A}$ output A map by control error $\Xi = \hat{A} - A$ for constant frequency S_V. We can say the controller is stabilizable for the noninvasive periodic solution and $u_2 \in S_V$ if the sequence of control error Ξ_k crosses zero for some A_k for constant frequency S_v.

Let us say we found a zero-crossing sequence of Ξ_k from the experiment, which means the controller is stabilizable and $u_2 \in S_V$ for some constant frequency S_v. Then, CBC scheme for this type of dynamical system can be summarized as Figure 1, where Δ is step size of $\hat{A}$ and δ is the zero tolerance of Ξ for finding a noninvasive periodic solution.

4. Experimental example

In this section, we show scheme developed in Section 3 can be applied to a real-world dynamical system with Hopf bifurcation. We applied the developed scheme to a flutter [30] rig, where flutter is one of the typical Hopf bifurcation problems in aerodynamics.

(a) Experiment setup

The experiment was performed on flutter rig with a NACA-0015 wing profile [31]. The profile moves in two degrees of freedom, heave, and pitch. Coil springs are installed to add linear stiffness to the heave and pitch motion, and spring plate is installed to add nonlinearity on the pitch stiffness. Measurements are

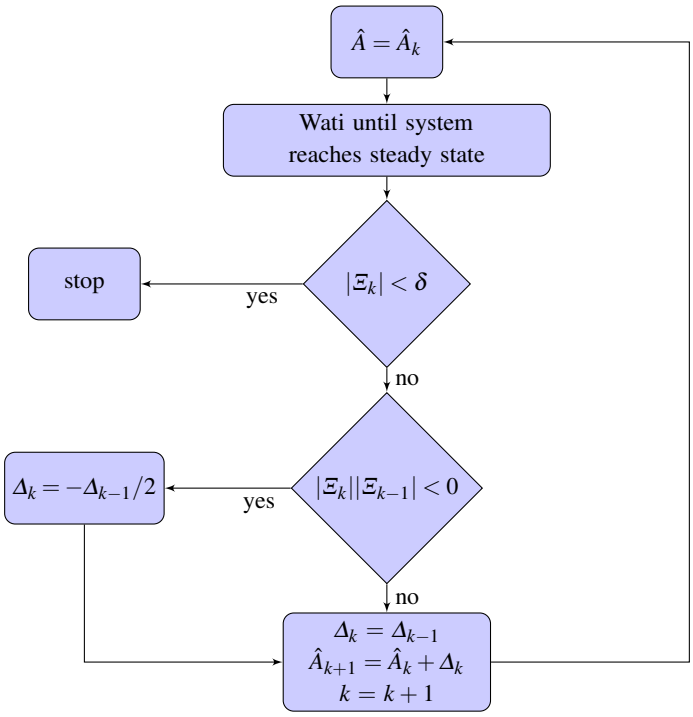

Figure 1: Flow chart diagram of finding noninvasive periodic solution

taken at shaft with digital encoder for pitch and heave motion was measured from laser displacement sensor. Data acquisition and real-time control were performed with Beaglebone Black and real-time controller [32]. Control force was applied to heave motion to stabilize unstable LCO with APS Electro-Seis Shaker and schematics of a configuration of the experiment and picture of the rig is presented in Figure 2.

(b) Experiment results

Open-loop tests are performed initially to investigate the dynamics of the system. Below the wind speed approximately 15 m/sec, equilibrium is stable and transient response ends with equilibrium state when the large perturbation is applied to equilibrium. However, above the wind speed approximately 15 m/sec, transient response ends with stable LCO when even small perturbation is applied to equilibrium. From this observation, we assume that the dynamical system has subcritical Hopf bifurcation and family of LCO has a fold at approximately around 15 m/sec.

To stabilize the unstable LCO, we first make multiple measurements at the different amplitude of control target to analyze the stabilizability. Figure 3 (a) shows that the variation of frequency is small when multiple measurements of phase-locked periodic orbit was taken with a different amplitude of target coefficient $\hat{A}$. Therefore, we assume that the measured phase-locked solution of this system is an element of constant frequency family of stable phase-locked solution. Stabilizability of the controller can be analyzed from error function Ξ. We conclude controller is stabilizable for the unstable LCO if the Ξ crosses zero as Figure 3 (b) for some sequence of $\hat{A}_k$.

Now, finding a noninvasive point to measure the unstable LCO is equivalent to solving zero problem of Ξ, which is a function of $\hat{A}$. Ξ has two zero points at unstable low amplitude LCO and stable high amplitude LCO. Figure 4 shows the time response of heave response and control target with zero tolerance $\delta = 1.8\,mm$, where we can find input and output is sufficiently identical and phase locking between the control target and the response is accomplished by the real-time controller. We assume the zero tolerance is sufficiently small that the measured unstable and stable LCO has the same amplitude and frequency with the LCO of

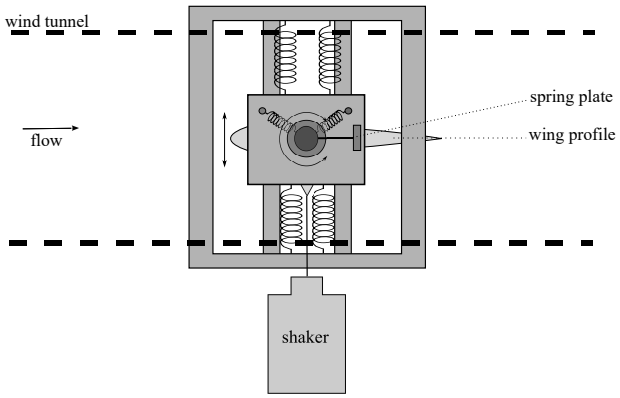

(a) Schematic of flutter rig

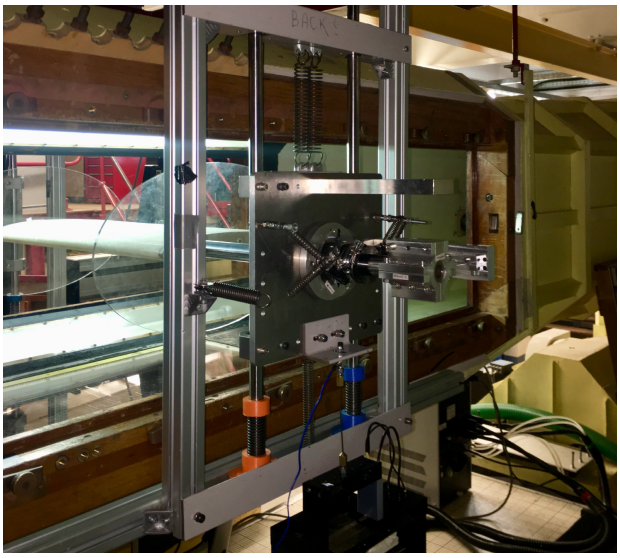

(b) Picture of flutter rig.

Figure 2: Schematic drawing and picture of flutter rig.

the uncontrolled system. This can be verified for the stable LCO by switching off the control as shown in Figure 5, stable LCO maintains it's motion; however, unstable LCO is attracted to stable equilibrium when the controller is turned off.

Noninvasive points were found experimentally to obtain a bifurcation diagram of this dynamical system. Results are presented in Figure 6, which shows the measured unstable LCO, stable LCO with different wind velocities. In this research, zero problems were not embedded in the pseudo arclength continuation since the wind speed of the wind tunnel was uncontrollable by the real-time controller. However, CBC scheme developed here can be embedded to pseudo arclength continuation if the real-time controller is able to control the unfolding parameter of the Hopf bifurcation.

5. Application of CBC for system identification

System identification is building a mathematical model from the results of an experiment which can provide valuable physical insights to researchers. We will show CBC can be utilized to verify the linearized dynamical model and used as a tool to identify the grey-box model [33] in this section. First, parameters associated

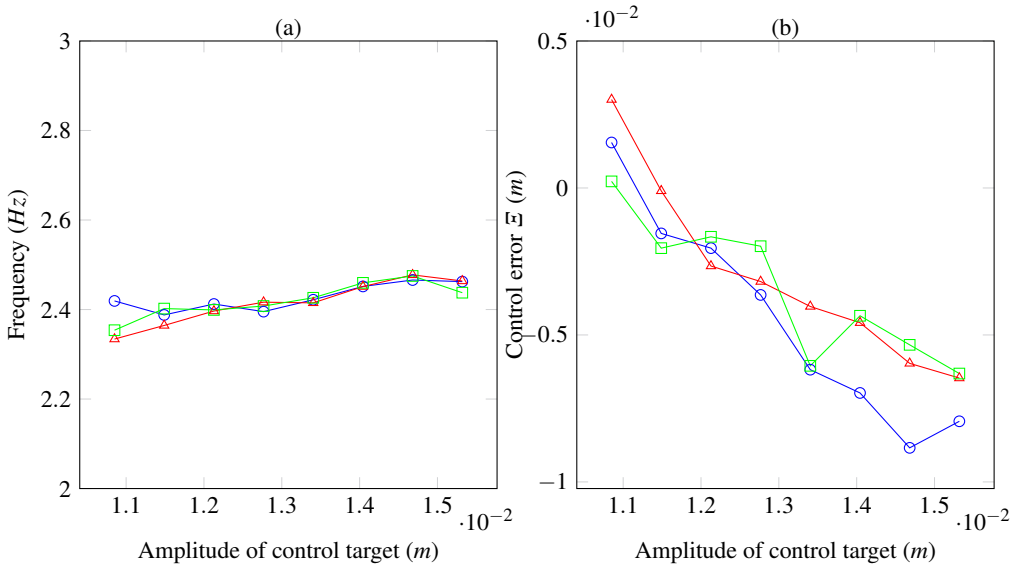

Figure 3: Multiple measurements of frequency and control error of phase locked periodic solutions at different amplitudes of control target (a) frequency, (b) error.

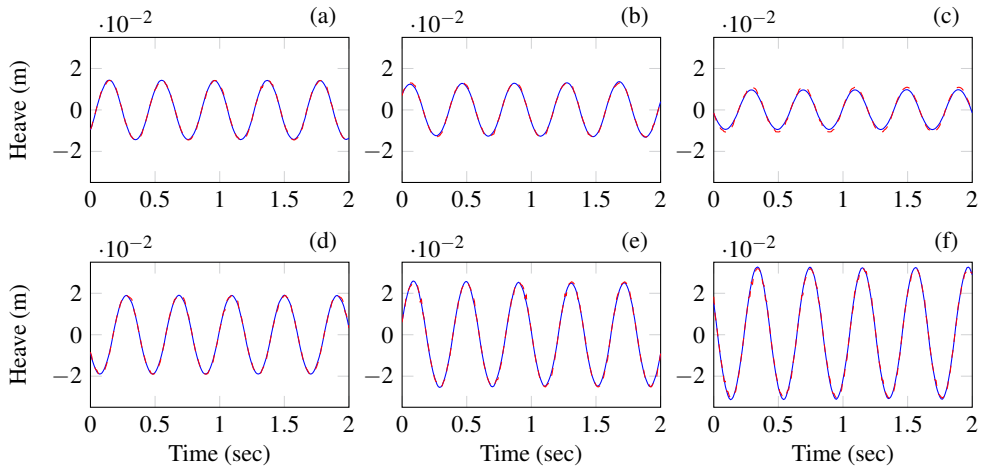

Figure 4: (a) Unstable LCO (U=14.9 m/sec), (b) Unstable LCO (U=15.6 m/sec), (c) Unstable LCO (U=16.5 m/sec), (d) Stable LCO (U=14.9 m/sec), (e) Stable LCO (U=15.6 m/sec), (f) Stable LCO (U=16.5 m/sec). (——) is the heave response of the rig, (- - -) is the control target.

with the linearized part of the equation of motion is identified with linear system identification method, and the Hopf point and Hopf frequency of the model is compared with the CBC results. Parameters associated with the nonlinear part of the equation of motion is identified using normal form theory to minimize the prediction error of the LCO amplitudes.

(a) Physical model for dynamical system

There are many physical models describing flutter; however, we use a simplified 2D model since the wing profile of the flutter rig has a simple shape. To take account of wake effects on the aerodynamic loads, we use

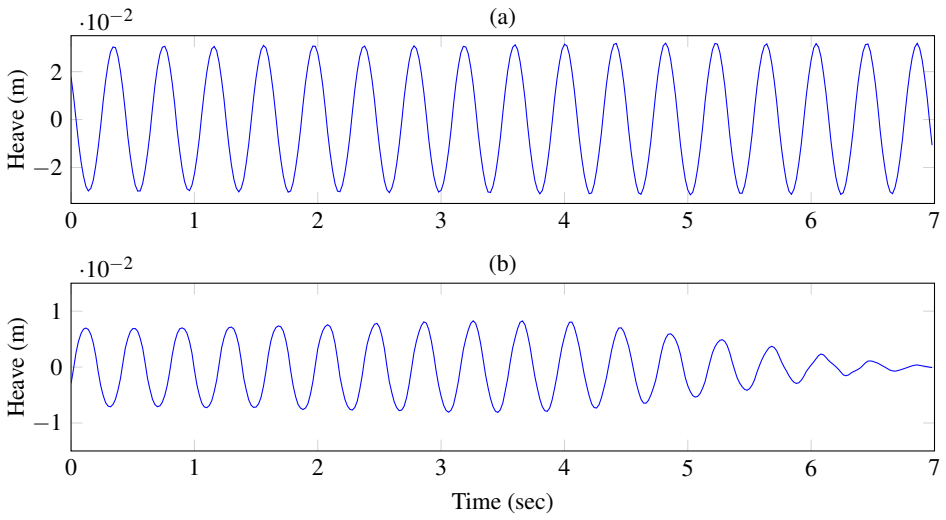

Figure 5: Response of the LCO after the controller truned off at $t = 3$ *sec* (a) Stable LCO ($U = 16.4\, m/sec$), (b) Untable LCO ($U = 16.4\, m/sec$).

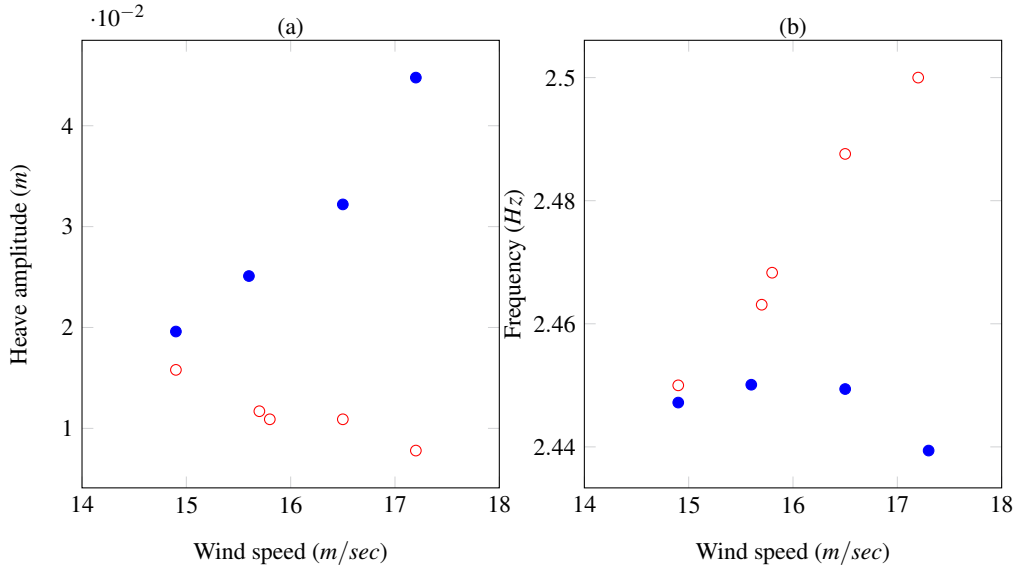

Figure 6: CBC results (a) Heave amplitude of LCO (m), (b) Frequeny of LCO (Hz). (●) is measured stable LCO and (○) is the measured unstable LCO.

unsteady formulation [34], which is much more accurate compared to quasi-static model [35]. The damping force of the system is assumed as linear viscous damping in both pitch and heave motion, and we assume that spring plate is the only source of nonlinearity in this system. We omit the detailed derivation of unsteady formulation, but a detailed explanation can be found in [34]. General equation of motion is,

$$\mathbf{M}\ddot{\mathbf{p}} + \mathbf{D}\dot{\mathbf{p}} + \mathbf{K_p}\mathbf{p} + \mathbf{N}(\mathbf{p}) = 0. \tag{5.1}$$

where,

$$\mathbf{p} = [h, \alpha, w]^T,\ \mathbf{N}(\mathbf{p}) = [0, k_{\alpha 2}\alpha^2 + k_{\alpha 3}\alpha^3, 0]^T, \tag{5.2}$$

$$\mathbf{M} = \begin{bmatrix} m_T + \pi\rho b^2 & mx_\alpha b - a\pi\rho b^3 & 0 \\ mx_\alpha b - a\pi\rho b^3 & I_\alpha + \pi(1/8 + a^2)\rho b^4 & 0 \\ 0 & 0 & 1 \end{bmatrix}, \tag{5.3}$$

$$\mathbf{D} = \begin{bmatrix} c_h + \pi\rho bU & (1 + (1/2 - a))\pi b^2 U & 2\pi U^2 b(c_1 c_2 + c_3 c_4) \\ -\pi(a + 1/2)\rho b^2 & c_\alpha + (1/4 - a^2)\pi rhob^3 U & -2\pi rhob^2 U^2 (a + 1/2)(c_1 c_2 + c_3 c_4) \\ -1/b & a - 1/2 & (c_2 + c_4)U/b \end{bmatrix}, \tag{5.4}$$

$$\mathbf{K} = \begin{bmatrix} k_h & \pi\rho bU^2 & 2\pi U^3 c_2 c_4 (c_1 + c_3) \\ 0 & k_\alpha - \pi(1/2 + a)\rho b^2 U^2 & -2\pi rhobU^3 (a + 1/2)(c_2 c_4 (c_1 + c_3)) \\ 0 & -U/b & c_2 c_4 U^2 / b^2 \end{bmatrix}. \tag{5.5}$$

w is an additional state variable introduced to express the aerodynamic force. Description of parameters used in (5.1) - (5.5) is presented in Table 3.2 and schematics of coordinate system of the unsteady formulation is given in Figure 7.

Table 1: Parameters of aeroelastic wing

Parameter	Description
b	Wing semi-chord (m)
a	Position of elastic axis relative to the semi-chord
ρ	Air density (m)
m_w	Mass of the wing (kg)
m_T	Mass of wing and support (kg)
I_α	Moment of inertia of wing about the elastic axis (kgm^2)
c_α	Linear damping coefficient of pitch motion (kgm^2/s)
c_h	Linear damping coefficient of pitch motion (kg/s)
k_α	Linear stiffness in pitch (N)
$k_{\alpha 2}$	Square nonlinear stiffness in pitch (N)
$k_{\alpha 3}$	Cubic nonlinear stiffness in pitch (N)
k_h	Linear stiffness in heave (N)
x_α	Nondimensional distance between center of gravity and elastic axis

If we express the equation of motion in state variable $\mathbf{z} = [h, \dot{h}, \alpha, \dot{\alpha}, w, \dot{w}]^T$, we obtain the following form:

$$\dot{\mathbf{z}} = \mathbf{B}(U)\mathbf{z} + \mathbf{N_0}(\mathbf{z}), \tag{5.6}$$

where, $\mathbf{B}(U)$ is the Jacobian of the equation of motion at the equilibruum ($\mathbf{z} = 0$) which can be computed by rearraging (5.1) - (5.5) to (5.6) , and $\mathbf{N_0}(\mathbf{z})$ is the nonlinear part of the equation which can be easilly trasformed from $\mathbf{N}(\mathbf{p})$.

(b) Parameter identification of the linearized model

For small-amplitude response, we can neglect the contribution of nonlinear function $\mathbf{N_0}$ from (5.6) and the system can be regarded as linear. Linear system parameter identification can be done with various existing methods, wavelet transform [36], frequency-domain methods [37], and state-space models [38]. State-space models provide a direct connection between measurable physical variables and the measured response,

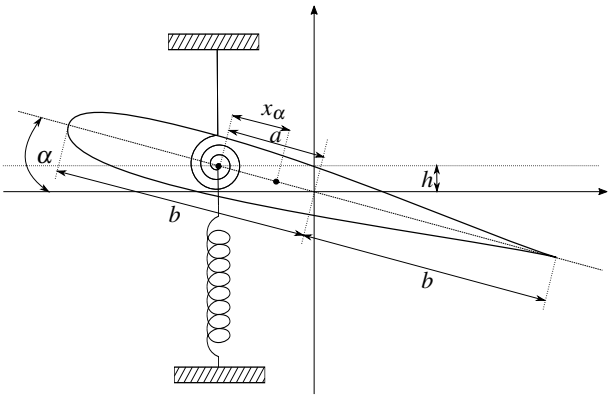

Figure 7: Schematic drawing of simplified aeroelastic model.

while other methods deal with modal properties. Therefore, we use the state-space model to identify the unknown parameters of the experimental rig from the free decay response at low amplitude without flow ($U = 0$). Wing semi- chord b, the position of the elastic axis relative to the semi-chord a, the mass of the wing m, the mass of the total wing structure including support m_T modal frequency of pitch $\omega_a = \sqrt{k_\alpha / I_\alpha}$, modal frequency of the heave $\omega_h = \sqrt{k_h / m_T}$, and nondimensional distance between center of gravity and elastic axis x_α are the coefficients that can be easilly measured. Air density ρ is known value and we set $\theta = [I_\alpha, c_\alpha, c_h, \dot{h}(0), \dot{\alpha}(0)]^T$ as unknown parameter vector which is much more difficult to measure compared to the known parameters. Note that $\dot{h}(0)$, $\dot{\alpha}(0)$ are initial value of unmeasured state variables which are unknown parameters. Since we only use free decay response for zero flow velocity, we rewrite Jacobian of (5.6) as function of unknown parameters $\mathbf{B}(\theta)$. State-space representation of linearized part of (5.6) can be represented as a finite difference equation when sampling time is T_s as

$$\begin{aligned} \mathbf{z}(k+1) =& \mathbf{A}_{T_s}(\theta)\mathbf{z}(k), \\ \mathbf{y} =& \mathbf{C}\mathbf{z} + \mathbf{w}, \end{aligned} \tag{5.7}$$

where, $\mathbf{C} = diag(1,0,1,0)$ is matrix that relates state variable and measured output$\mathbf{y}$, $\mathbf{w}$ is measurement noise, and $\mathbf{A}_{T_s}$ can be computed as

$$\mathbf{A}_{T_s}(\theta) = e^{\mathbf{B}(\theta)T_s}. \tag{5.8}$$

To identify the unknown parameters, we use prediction-error identification methods [38]. Prediction error $\hat{\varepsilon}$ can be defined as

$$\hat{\varepsilon}(k,\theta) = \mathbf{y}(k) - \hat{\mathbf{y}}(k|\theta), \tag{5.9}$$

where, $\hat{\mathbf{y}}(k|\theta)$ is predicted response from (3.30). Parameters that minimize the prediction error $\hat{\theta}$ can be estimated by

$$\hat{\theta} = \underset{\theta \in D_m}{\arg\min}\, V_N(\theta, \mathbf{Z}^N), \tag{5.10}$$

where, D_m is vector space of unknown parameters, V_N is the summation of vector norm of filtered prediction error, N is the length of the free-decay data, and $\mathbf{Z}^N$ is a vector containing all measured signal. See [38] for details about the filter and the algorithm. Values of identified parameters and measured parameters are given in Table 2.

The identified linearized model can be verified by comparing flutter speed and flutter frequency obtained from CBC results. If we use Assumption 3.1, the square of LCO amplitude is proportional to the unfolding

Table 2: Values of parameters of linearized model

Measured Parameter	Value	Identified parameter	Value
b	0.15 m	I_α	0.1724 kgm^2
a	-0.5	c_α	0.5628 kgm^2/s^2
ρ	1.204 kg/m^3	c_h	14.5756 kg/s
k_h	3529.4 N/m	k_α	54.11 N
m_w	5.3 kg		
m_T	16.9 kg		
x_α	0.24		

parameter. Therefore, we can estimate the flutter speed from the linear regression of the square of LCO amplitude crosses zero (Figure 8 (a)), and flutter frequency can be estimated from the relation between the unfolding parameter and the frequency of the LCO from (3.10) which is a linear function if we truncate the normal form to the third order (Figure 8 (b)).

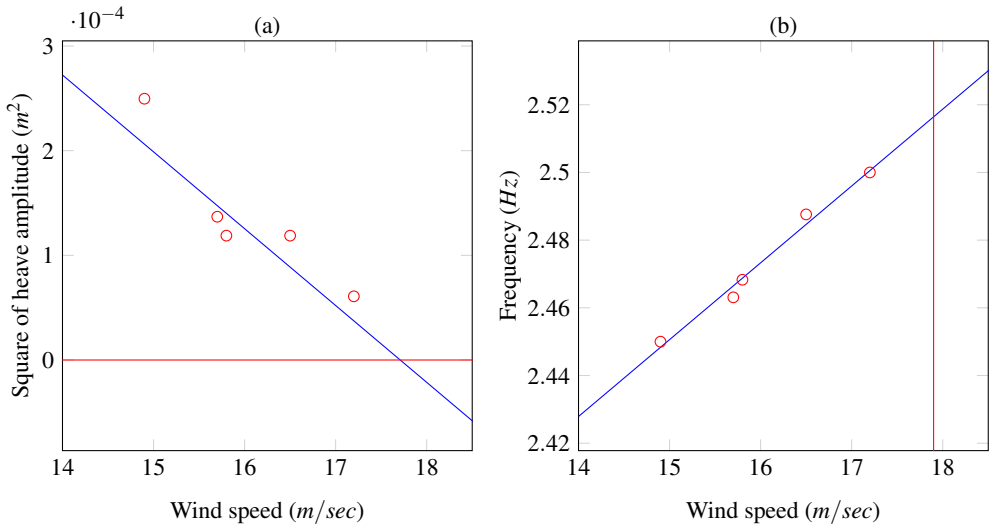

Figure 8: Estimation of flutter properties based on normal form (a) flutter speed estimation (U_0 = 17.9 m/sec), (b) flutter frequeny estimation (f_0 = 2.51 Hz). (——) is linear regression curve of measured square of heave amplitude, and (○) is the measured square of heave amplitdue.

If we see the computed eigenvalues of the Jacobian of the identified linearized system (Figure 9), the comparison between the estimated values from the model and measured values is possible. Note that two eigenvalues with zero imaginary part is neglected in Figure 9 which are unable to measure during the zero wind speed. Estimated futter speed from the model is 17.96 m/s and measured futter speed is 17.89 m/s. Estimated futter frequency from the model is 2.46 Hz measured flutter frequency is 2.51 Hz, which is quite close enough to say identified linearized dynamical model is sufficiently accurate.

(c) Parameter identification of the nonlinear model

If we define $\mu = U_f - U$ and insert $U = U_f - \mu$ to (5.6), where U_f is the flutter speed, (5.6) has codim-1 Hopf bifurcation at $\mu = 0$. First, (5.6) should be expressed in the form of (3.2) by adding $\dot{\mu} = 0$ to the equation of motion. Then, 3-dimensional center manifold and reduced dynamics on the center manifold can be computed from (3.3). We used symbolic computational program Maple^{TM} [39] to compute the center manifold and

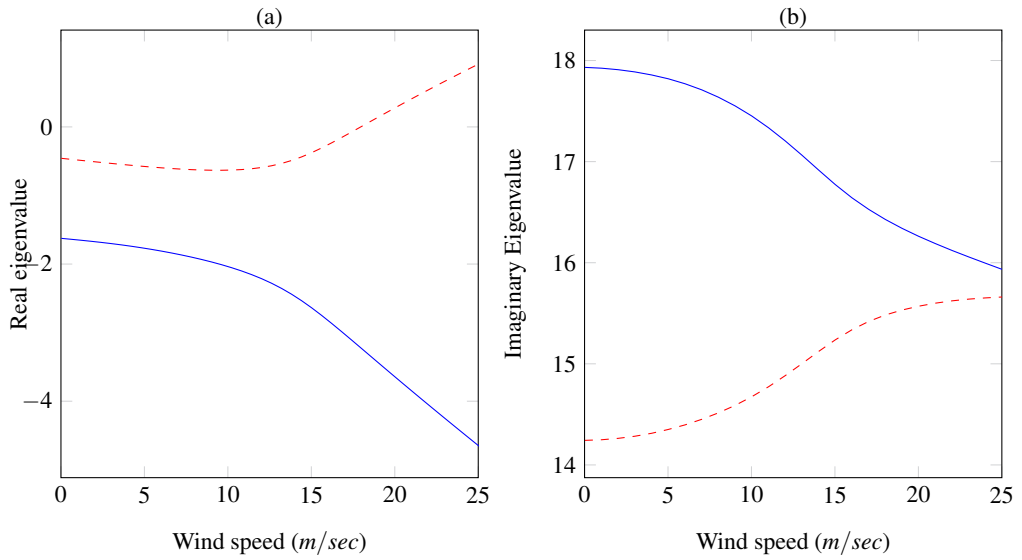

Figure 9: Eigenvalues of identified linearized system (a) real eigenvalue, (b) imaginary eigenvalue. (——) is mode 1 and (- - -) is mode 2.

normal form. Results of center manifold and reduced dynamics of (5.6) is presented in Appendix A.

SNF of (5.6) can be computed by inserting (3.6) to the reduced dynamics and solving (3.7) at second and third order. SNF in polar coordinates is

$$\begin{aligned}\frac{dR}{d\tau} &= 0.0075\nu R + (-5.88\times10^{-6}k_{\alpha3} + 6.72\times10^{-9}k_{\alpha2}^2)R^3 \\ \frac{d\Theta}{d\tau} &= (8.57\times10^{-10}k_{\alpha2}^2) - 2.61\times10^{-6}k_{\alpha3},\end{aligned} \tag{5.11}$$

where details of nonlinear transformation is given in Appendix B. Amplitude of LCO is now function of nonlinear parameters $k_{\alpha2}$, $k_{\alpha3}$, and unfolding parameter ν which is a nonzero equilibria of (5.11)

$$R = \frac{0.0075\nu}{-5.88\times10^{-6}k_{\alpha3} + 6.72\times10^{-9}k_{\alpha2}^2}. \tag{5.12}$$

We define prediction error of LCO amplitude by

$$\hat{V}(\theta_n) = \sum_M (R(\nu_M, \theta_n) - R_m)^2, \tag{5.13}$$

where M is index of measurement points of CBC, R_m is measured amplitude of LCO, and $\theta_n = [k_{\alpha2}, k_{\alpha3}]^T$ is vector of unknown nonlinear parameters. Note that normal form theory is valid only at unstable LCOs since topological equivalence cannot be provided by nonlinear transformations (3.6) after the fold point; therefore, only unstable LCO results are used. These parameters can be estimated similarly with linearized system identification by

$$\begin{aligned}\hat{\theta}_n &= \underset{\theta_n \text{ s.t. } S>0}{\arg\min}\ \hat{V}(\theta_n), \\ S &= -5.88\times10^{-6}k_{\alpha3} + 6.72\times10^{-9}k_{\alpha2}^2,\end{aligned} \tag{5.14}$$

where $S > 0$ is the constraint to keep the type of Hopf bifurcation to subcritical which is our experimental case. Solving (5.14), we heave

$$k_{\alpha 2} = 2936.3\,Nm,\ k_{\alpha 3} = 795.3\,Nm. \tag{5.15}$$

For the validation of the results, we compare estimated amplitude via numerical continuation, normal form, and measured amplitude in Figure 10. Numerical continuation results are carried out with coco [16]. Measured heave amplitude and computed heave amplitude from the numerical continuation is in good agreement. Less accurate agreement for pitch between the measurement and numerical continuation is due to the inaccuracy of the estimated modal vector from the linearized model and the inaccuracy of the normal form far from the Hopf point. Accuracy of the modal vector can be improved by using input signals such as random excitation in a linear state-space model, and accuracy of the normal form can be increased by taking higher-order approximation. However, improving the accuracy of the identified model is not the scope of this paper. Also, the identified model show poor agreement in the stable branch of LCO with measurement results, and the reason is not identified yet, which we leave it for future research.

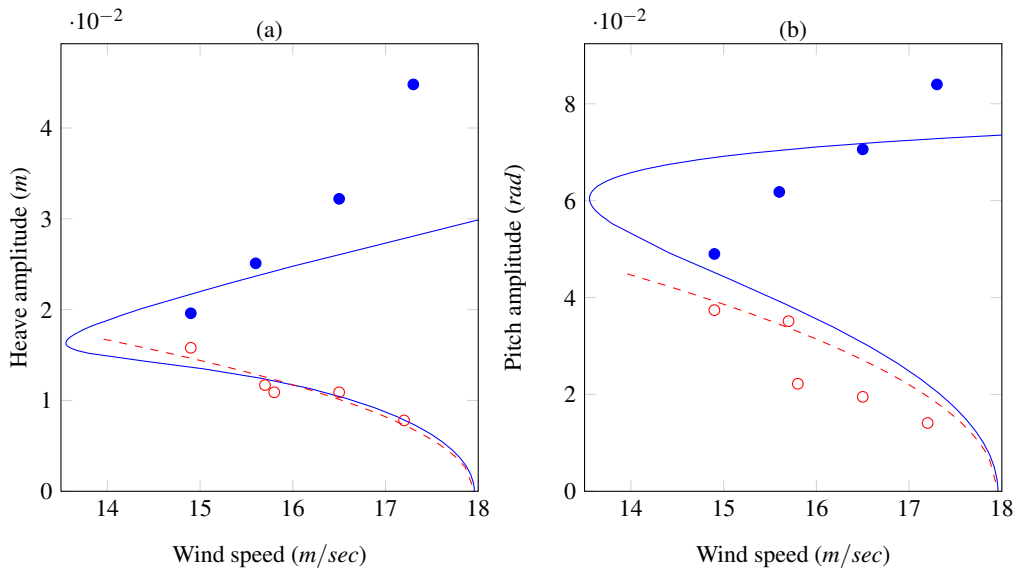

Figure 10: Comparison between measured and Computed amplitude of limit cycle. (a) Heave amplitude (b) Pitch amplitude. (——) is computed amplitude by numerical continuation, (- - -) is computed amplitude by normal form, (●) is measured stable limit cycle, and (○) is measured unstable limit cycle.

6. Conclusion

CBC scheme for stabilizing unstable LCOs near Hopf bifurcation is developed. A dynamical system with CBC can be simplified to a Hopf bifurcation with single harmonic forcing if weakly nonlinear transformation is assumed during normal form derivation. Input-output map of CBC for Hopf bifurcation can be defined as a one-dimensional map if the response of the controlled system is an element of constant frequency family of phase-locked periodic solution and phase-locking between the control target and the response is forced by the real-time controller. Therefore, finding a noninvasive periodic solution is equivalent to finding a zero solution of the control error function. Developed CBC scheme is applied to a flutter rig, and unstable LCO was stabilized at five different wind speed. This result can be applied to verify the identified linearized dynamical model and utilized as an identification tool of the grey-box model.

To apply CBC to more general Hopf bifurcation problems, frequency of the phase-locked periodic solutions in (3.29) should be controllable. Also, a methodology to decrease the influence of the measurement noise should be considered to increase the accuracy of the CBC results.

Data Accessibility. Insert data access text here.

Authors' Contributions. All authors contributed to the formation and fundamental concepts of the research. D.A.W.B. developed the phase-locked CBC scheme and the exprimental setup. L.R. assisted on experimental data analysis and system identification. All authors contributed to the preparation of the manuscript.

Competing Interests. We have no competing interests

Funding. Insert funding text here.

Acknowledgements. Insert acknowledgment text here.

Appendix A. Center manifold and reduced dynamics of (5.6)

Jordan normal form of (5.6) can be derived as

$$\dot{X} = JX + \Sigma^{-1}\mathbf{N}_0(\Sigma X), \tag{Appendix A.1}$$

where, Σ is coordinate transformation matrix whose columns are eigenvectors of eigenvalues of $\mathbf{B}(U)$ and satisfies $\mathbf{J} = \Sigma^{-1}\mathbf{B}(U)\Sigma$

$$\mathbf{J} = \begin{bmatrix} 15.48\mathrm{i} & 0 & 0 & 0 & 0 & 0 \\ 0 & -15.48\mathrm{i} & 0 & 0 & 0 & 0 \\ 0 & 0 & -3.22+16.43\mathrm{i} & 0 & 0 & 0 \\ 0 & 0 & 0 & -3.22-16.43\mathrm{i} & 0 & 0 \\ 0 & 0 & 0 & 0 & -35.42 & 0 \\ 0 & 0 & 0 & 0 & 0 & -5.4133 \end{bmatrix}, \tag{Appendix A.2}$$

Let $\mathbf{x} = [x, \bar{x}]^T$ be the centerspace at $\mu = U - U_f = 0$ and $\mathbf{y} = [y_1, y_2, y_3, y_4]^T$ be the stable eigenspace of (5.6), where $\mathbf{X} = [\mathbf{x}, \mathbf{y}]^T$. Coefficeins of power series of centermanifold can be computed by solving (3.2) every order. See [22] for detailed effective algorithm for solving coefficients recursively. Centermanifold $\mathbf{y} = \mathbf{H}(\mathbf{x}, \mu)$ of (3.2) can be computed upto third order as

$$\begin{aligned} y_1 =& (-0.00208 + 0.00245\,i)\mu^2 x + (0.000114 - 0.000117\,i)\mu^2\bar{x} + (0.264 - 1.02\,i)\times \\ & (0.00000172\,ik_{\alpha 2} + 0.000000772\,k_{\alpha 2})\mu\, x^2 + (0.193 + 0.882\,i)(-0.00000455\,k_{\alpha 2} - 0.00000315\,ik_{\alpha 2})\mu\, x\bar{x} \\ & + (0.0248 + 0.323\,i)(0.0000000969\,ik_{\alpha 2} + 0.00000292\,k_{\alpha 2})\mu\,\bar{x}^2 + (0.0635 - 0.513\,i)\times \\ & (0.00000196\,k_{\alpha 3} - 0.00000000226\,{k_{\alpha 2}}^2 - 0.000000654\,ik_{\alpha 3} - 0.00000000199\,i{k_{\alpha 2}}^2)x^3 + \\ & (3.77 + 1.30\,i)(0.00000262\,ik_{\alpha 3} + 0.00000000900\,i{k_{\alpha 2}}^2 0.00000588\,k_{\alpha 3} + 0.0000000108\,{k_{\alpha 2}}^2)\times x^2\bar{x} + \\ & (0.0540 + 0.474\,i)(-0.00000262\,ik_{\alpha 3} - 0.00000000522\,i{k_{\alpha 2}}^2 + 0.00000588\,k_{\alpha 3} - 0.00000000588\,{k_{\alpha 2}}^2) \\ & x\bar{x}^2 + (0.0142 + 0.244\,i)(-0.00000196\,k_{\alpha 3} - 0.00000000274\,{k_{\alpha 2}}^2 - 0.00000000163\,i{k_{\alpha 2}}^2 + \\ & 0.000000654\,ik_{\alpha 3})\bar{x}^3 - (0.0202 + 0.0419\,i)\mu\, x - (0.00325 - 0.00293\,i)\mu\,\bar{x} + (0.264 - 1.02\,i)\times \\ & (-0.0000163\,k_{\alpha 2} - 0.0000314\,ik_{\alpha 2})x^2 + (0.193 + 0.882\,i)(0.0000320\,k_{\alpha 2} + 0.0000634\,ik_{\alpha 2})x\bar{x} + \\ & (0.0248 + 0.323\,i)(-0.0000163\,k_{\alpha 2} - 0.0000314\,ik_{\alpha 2})\bar{x}^2, \end{aligned} \tag{Appendix A.3}$$

$$y_2 = (0.000114 + 0.000117\,i)\mu^2 x - (0.00208 + 0.00245\,i)\mu^2 \bar{x} + (0.0248 - 0.323\,i)(-0.00000163\,k_{\alpha 2} + 0.00000244\,ik_{\alpha 2})\mu x^2 + (0.193 - 0.882\,i)(-0.00000551\,ik_{\alpha 2} + 0.000000118\,k_{\alpha 2})\mu x\bar{x} + (0.264 + 1.02\,i)\times(0.000000957\,k_{\alpha 2} + 0.00000167\,ik_{\alpha 2})\mu \bar{x}^2 + (0.0142 - 0.244\,i)(0.00000196\,k_{\alpha 3} + 0.00000000243\,{k_{\alpha 2}}^2 - 0.000000654\,ik_{\alpha 3} + 0.00000000209\,i{k_{\alpha 2}}^2)x^3 + (0.0540 - 0.474\,i)(0.00000262\,ik_{\alpha 3} - 0.00000588\,k_{\alpha 3} + 0.00000000379\,i{k_{\alpha 2}}^2 + 0.00000000691\,{k_{\alpha 2}}^2)x^2\bar{x} + (3.77 - 1.30\,i)(-0.00000262\,ik_{\alpha 3} - 0.00000000749\,i{k_{\alpha 2}}^2 + 0.00000588\,k_{\alpha 3} - 0.0000000119\,{k_{\alpha 2}}^2)x\bar{x}^2 + (0.0635 + 0.513\,i)(-0.00000196\,k_{\alpha 3} + 0.00000000263\,{k_{\alpha 2}}^2 + 0.00000000146\,i{k_{\alpha 2}}^2 + 0.000000654\,ik_{\alpha 3})\bar{x}^3 - (0.00325 + 0.00293\,i)\mu x - (0.0202 - 0.0419\,i)\mu \bar{x} + (0.0248 - 0.323\,i)\times(-0.0000163\,k_{\alpha 2} - 0.0000314\,ik_{\alpha 2})x^2 + (0.193 - 0.882\,i)\times(0.0000320\,k_{\alpha 2} + 0.0000634\,ik_{\alpha 2})x\bar{x} + (0.264 + 1.02\,i)(-0.0000163\,k_{\alpha 2} - 0.0000314\,ik_{\alpha 2})\bar{x}^2,$$

(Appendix A.4)

$$y_3 = (0.000150 + 0.000122\,i)\mu^2 x + (0.000150 - 0.000122\,i)\mu^2 \bar{x} + (0.240 - 0.180\,i)(0.00000241\,ik_{\alpha 2} + 0.00000399\,k_{\alpha 2})\mu x^2 + (0.375 - 0.0\,i)(-0.0000156\,k_{\alpha 2} - 0.0000309\,ik_{\alpha 2})\mu x\bar{x} + (0.240 + 0.180\,i)\times(0.00000469\,ik_{\alpha 2} - 0.000000325\,k_{\alpha 2})\mu \bar{x}^2 + (0.166 - 0.186\,i)(0.00000196\,k_{\alpha 3} + 0.000000000962\,{k_{\alpha 2}}^2 - 0.000000654\,ik_{\alpha 3} + 0.000000000926\,i{k_{\alpha 2}}^2)x^3 + (0.329 - 0.123\,i)(0.00000262\,ik_{\alpha 3} + 0.00000000407\,i{k_{\alpha 2}}^2 - 0.00000588\,k_{\alpha 3} + 0.00000000599\,{k_{\alpha 2}}^2)x^2\bar{x} + (0.329 + 0.123\,i)(-0.00000262\,ik_{\alpha 3} - 0.00000000438\,i{k_{\alpha 2}}^2 + 0.00000588\,k_{\alpha 3} - 0.00000000575\,{k_{\alpha 2}}^2)x\bar{x}^2 + (0.166 + 0.186\,i)(-0.00000196\,k_{\alpha 3} - 0.00000000119\,{k_{\alpha 2}}^2 - 0.000000000617\,i{k_{\alpha 2}}^2 + 0.000000654\,ik_{\alpha 3})\bar{x}^3 - (0.00186 - 0.00128\,i)\mu x - (0.00186 + 0.00128\,i)\mu \bar{x} + (0.240 - 0.180\,i)(-0.0000163\,k_{\alpha 2} - 0.0000314\,ik_{\alpha 2})x^2 + (0.375 - 0.0\,i)\times(0.0000320\,k_{\alpha 2} + 0.0000634\,ik_{\alpha 2})x\bar{x} + (0.240 + 0.180\,i)(-0.0000163\,k_{\alpha 2} - 0.0000314\,ik_{\alpha 2})\bar{x}^2,$$

(Appendix A.5)

$$y_4 = (0.0000561 - 0.0000151\,i)\mu^2 x + (0.0000561 + 0.0000151\,i)\mu^2 \bar{x} + (0.0976 - 0.480\,i)(0.00000355\,ik_{\alpha 2} + 0.00000107\,k_{\alpha 2})\mu x^2 + (2.46 - 0.0\,i)(-0.00000989\,ik_{\alpha 2} - 0.00000502\,k_{\alpha 2})\mu x\bar{x} + (0.0976 + 0.480\,i)\times(0.00000295\,ik_{\alpha 2} + 0.00000225\,k_{\alpha 2})\mu \bar{x}^2 + (0.0444 - 0.327\,i)(0.00000196\,k_{\alpha 3} - 0.00000000292\,{k_{\alpha 2}}^2 - 0.000000654\,ik_{\alpha 3} + 0.00000000504\,i{k_{\alpha 2}}^2)x^3 + (0.349 - 0.858\,i)(0.00000262\,ik_{\alpha 3} - 0.00000588\,k_{\alpha 3} + 0.000000000884\,i{k_{\alpha 2}}^2 + 0.0000000112\,{k_{\alpha 2}}^2)x^2\bar{x} + (0.349 + 0.858\,i)(-0.00000262\,ik_{\alpha 3} - 0.0000000102\,i{k_{\alpha 2}}^2 + 0.00000588\,k_{\alpha 3} - 0.00000000419\,{k_{\alpha 2}}^2)x\bar{x}^2 + (0.0444 + 0.327\,i)(-0.00000196\,k_{\alpha 3} - 0.00000000384\,{k_{\alpha 2}}^2 + 0.00000000436\,i{k_{\alpha 2}}^2 + 0.000000654\,ik_{\alpha 3})\bar{x}^3 + (0.00000808 + 0.000696\,i)\mu x + (0.00000808 - 0.000696\,i)\mu \bar{x} + (0.0976 - 0.480\,i)\times(-0.0000163\,k_{\alpha 2} - 0.0000314\,ik_{\alpha 2})x^2 + (2.46 - 0.0\,i)\times(0.0000320\,k_{\alpha 2} + 0.0000634\,ik_{\alpha 2})x\bar{x} + (0.0976 + 0.480\,i)\times(-0.0000163\,k_{\alpha 2} - 0.0000314\,ik_{\alpha 2})\bar{x}^2.$$

(Appendix A.6)

Reduced dynamic on the centermanifold can be computed by inserting $\mathbf{y} = \mathbf{H}(\mathbf{x}, \mu)$ to (Appendix A.1) and collecting the first two equations as

$$\begin{aligned}\dot{x} =& 15.3ix - 0.125\bar{x}\mu - 0.0563i\bar{x}\mu - 0.000249k_{\alpha 2}\bar{x}^2 - 0.000480ik_{\alpha 2}\bar{x}^2 + 0.115x\mu + 0.0571ix\mu + \\ & 0.000970ik_{\alpha 2}x\bar{x} + 0.000490k_{\alpha 2}x\bar{x} - 0.000249k_{\alpha 2}x^2 - 0.000480ik_{\alpha 2}x^2 + 0.00203\bar{x}\mu^2 - 0.00453i\bar{x}\mu^2 + \\ & 0.00000233ik_{\alpha 2}\bar{x}^2\mu + 0.0000381k_{\alpha 2}\bar{x}^2\mu - 0.0000000208{k_{\alpha 2}}^2\bar{x}^3 - 0.0000000176i{k_{\alpha 2}}^2\bar{x}^3 - \\ & 0.0000300k_{\alpha 3}\bar{x}^3 + 0.0000100ik_{\alpha 3}\bar{x}^3 + 0.00223x\mu^2 - 0.00415ix\mu^2 + 0.00000171k_{\alpha 2}x\bar{x}\mu - \\ & 0.0000361ik_{\alpha 2}x\bar{x}\mu - 0.0000000508i{k_{\alpha 2}}^2x\bar{x}^2 - 0.0000000744{k_{\alpha 2}}^2x\bar{x}^2 - 0.0000401ik_{\alpha 3}x\bar{x}^2 + \\ & 0.0000900k_{\alpha 3}x\bar{x}^2 + 0.0000442ik_{\alpha 2}x^2\mu - 0.0000245k_{\alpha 2}x^2\mu + 0.0000000545i{k_{\alpha 2}}^2x^2\bar{x} + \\ & 0.0000000716{k_{\alpha 2}}^2x^2\bar{x} + 0.0000401ik_{\alpha 3}x^2\bar{x} - 0.0000900k_{\alpha 3}x^2\bar{x} + 0.0000000236{k_{\alpha 2}}^2x^3 + \\ & 0.0000000140i{k_{\alpha 2}}^2x^3 + 0.0000300k_{\alpha 3}x^3 - 0.0000100ik_{\alpha 3}x^3,\end{aligned} \tag{Appendix A.7}$$

$$\begin{aligned}\dot{\bar{x}} =& -15.3i\bar{x} + 0.115\bar{x}\mu - 0.0571i\bar{x}\mu - 0.000249k_{\alpha 2}\bar{x}^2 - 0.000480ik_{\alpha 2}\bar{x}^2 - 0.125x\mu + 0.0563ix\mu + \\ & 0.000970ik_{\alpha 2}x\bar{x} + 0.000490k_{\alpha 2}x\bar{x} - 0.000249k_{\alpha 2}x^2 - 0.000480ik_{\alpha 2}x^2 + 0.00223\bar{x}\mu^2 + 0.00415i\bar{x}\mu^2 + \\ & 0.00000586ik_{\alpha 2}\bar{x}^2\mu + 0.0000502k_{\alpha 2}\bar{x}^2\mu - 0.0000300k_{\alpha 3}\bar{x}^3 - 0.0000000208{k_{\alpha 2}}^2\bar{x}^3 + 0.0000100ik_{\alpha 3}\bar{x}^3 - \\ & 0.0000000176i{k_{\alpha 2}}^2\bar{x}^3 + 0.00203x\mu^2 + 0.00453ix\mu^2 - 0.0000306k_{\alpha 2}x\bar{x}\mu - 0.0000197ik_{\alpha 2}x\bar{x}\mu \\ & - 0.0000401ik_{\alpha 3}x\bar{x}^2 - 0.0000000508i{k_{\alpha 2}}^2x\bar{x}^2 + 0.0000900k_{\alpha 3}x\bar{x}^2 - 0.0000000744{k_{\alpha 2}}^2x\bar{x}^2 + \\ & 0.0000323ik_{\alpha 2}x^2\mu - 0.0000205k_{\alpha 2}x^2\mu + 0.0000401ik_{\alpha 3}x^2\bar{x} + 0.0000000545i{k_{\alpha 2}}^2x^2\bar{x} \\ & - 0.0000900k_{\alpha 3}x^2\bar{x} + 0.0000000716{k_{\alpha 2}}^2x^2\bar{x} + 0.0000300k_{\alpha 3}x^3 + 0.0000000236{k_{\alpha 2}}^2x^3 - \\ & 0.0000100ik_{\alpha 3}x^3 + 0.0000000140i{k_{\alpha 2}}^2x^3.\end{aligned} \tag{Appendix A.8}$$

Appendix B. Nonlinear transformations for SNF of (5.6) on the center manifold

Reduced dynamics (Appendix A.7),(Appendix A.8) can be transformed to (5.11) if we use (3.6), and the coefficients of nonlinear transformation can be computed by solving (3.7). From Assumption 3.1, we assume $C_{1ijk} = C_{2ijk=0}$ for $i + j \geq 0$, and we can have

$$C_{1101} = C_{2101} = C_{1011} = C_{2011} = 0, \tag{Appendix B.1}$$

and coefficients for time, parameter rescailing can be obtained as

$$p_2 = 2.19 \times 10^{-6}, \tag{Appendix B.2}$$

$$t_{10} = t_{11} = 0 = t_{20} = 0,\ t_{01} = -0.0037,\ t_{02} = 0.000016. \tag{Appendix B.3}$$

References

1. Pyragas K. Delayed feedback control of chaos. Philosophical Transactions of the Royal Society A: Mathematical, Physical and Engineering Sciences. 2006;364(1846):2309–2334.
2. Sieber J. Generic stabilizability for time-delayed feedback control. Proceedings of the Royal Society A: Mathematical, Physical and Engineering Sciences. 2016;472(2189):20150593.
3. Sieber J, Krauskopf B. Control based bifurcation analysis for experiments. Nonlinear Dynamics. 2008;51(3):365–377.

4. Sieber J, Krauskopf B, Wagg D, Neild S, Gonzalez-Buelga A. Control-based continuation of unstable periodic orbits. Journal of Computational and Nonlinear Dynamics. 2011;6(1):011005.
5. Bureau E, Schilder F, Santos IF, Thomsen JJ, Starke J. Experimental bifurcation analysis of an impact oscillator—tuning a non-invasive control scheme. Journal of Sound and Vibration. 2013;332(22):5883–5897.
6. Bureau E, Schilder F, Elmegård M, Santos IF, Thomsen JJ, Starke J. Experimental bifurcation analysis of an impact oscillator—Determining stability. Journal of Sound and Vibration. 2014;333(21):5464–5474.
7. Barton DA, Sieber J. Systematic experimental exploration of bifurcations with noninvasive control. Physical Review E. 2013;87(5):052916.
8. Barton DA, Burrow SG. Numerical continuation in a physical experiment: investigation of a nonlinear energy harvester. Journal of Computational and Nonlinear Dynamics. 2011;6(1):011010.
9. Renson L, Shaw A, Barton D, Neild S. Application of control-based continuation to a nonlinear structure with harmonically coupled modes. Mechanical Systems and Signal Processing. 2019;120:449–464.
10. Renson L, Gonzalez-Buelga A, Barton D, Neild S. Robust identification of backbone curves using control-based continuation. Journal of Sound and Vibration. 2016;367:145–158.
11. Renson L, Barton D, Neild S. Experimental analysis of a softening-hardening nonlinear oscillator using control-based continuation. In: Nonlinear Dynamics, Volume 1. Springer; 2016. p. 19–27.
12. Barton DA. Control-based continuation: Bifurcation and stability analysis for physical experiments. Mechanical Systems and Signal Processing. 2017;84:54–64.
13. Yu P, Leung A. The simplest normal form of Hopf bifurcation. Nonlinearity. 2002;16(1):277.
14. Ashwin P, Böhmer K, Mei Z. A numerical Liapunov-Schmidt method with applications to Hopf bifurcation on a square. Mathematics of computation. 1995;64(210):649–670.
15. Doedel EJ, Paffenroth RC, Champneys AR, Fairgrieve TF, Kuznetsov YA, Oldeman BE, et al. AUTO2000: Continuation and bifurcation software for ordinary differential equations. Report, Applied Mathematics, Caltech, Pasadena. 2000;.
16. Dankowicz H, Schilder F. Recipes for continuation. vol. 11. SIAM; 2013.
17. Brown G, Postlethwaite CM, Silber M. Time-delayed feedback control of unstable periodic orbits near a subcritical Hopf bifurcation. Physica D: Nonlinear Phenomena. 2011;240(9-10):859–871.
18. Postlethwaite C, Brown G, Silber M. Feedback control of unstable periodic orbits in equivariant Hopf bifurcation problems. Philosophical Transactions of the Royal Society A: Mathematical, Physical and Engineering Sciences. 2013;371(1999):20120467.
19. Golubitsky M, Shiau L, Postlethwaite C, Zhang Y. The feed-forward chain as a filter-amplifier motif. In: Coherent behavior in neuronal networks. Springer; 2009. p. 95–120.
20. Carr J. Applications of centre manifold theory. vol. 35. Springer Science & Business Media; 2012.
21. Kuznetsov YA. Elements of applied bifurcation theory. vol. 112. Springer Science & Business Media; 2013.
22. Bi Q, Yu P. Symbolic computation of normal forms for semi-simple cases. Journal of Computational and Applied Mathematics. 1999;102(2):195–220.
23. Algaba A, Freire E, Gamero E. Hypernormal form for the Hopf-zero bifurcation. International Journal of Bifurcation and Chaos. 1998;8(10):1857–1887.
24. Yu P. Computation of normal forms via a perturbation technique. Journal of Sound and Vibration. 1998;211(1):19–38.
25. Golubitsky M, Postlethwaite C. Feed-forward networks, center manifolds, and forcing. Discrete Contin Dyn Syst. 2012;32(8):2913–35.
26. Elphick C, Iooss G, Tirapegui E. Normal form reduction for time-periodically driven differential equations. Physics Letters A. 1987;120(9):459–463.
27. Zhang Y, Golubitsky M. Periodically forced Hopf bifurcation. SIAM Journal on Applied Dynamical Systems. 2011;10(4):1272–1306.
28. Wiser J, Golubitsky M. Bifurcations in forced response curves. SIAM Journal on Applied Dynamical Systems. 2015;14(4):2013–2029.
29. Tartaruga I. Experimental Identification of Unstable LCOs in a Wing Profile. NODYCON 2019 PROCEEDINGS. 2019;.
30. Dimitriadis G. Introduction to Nonlinear Aeroelasticity. John Wiley & Sons; 2017.
31. Jacobs EN, Ward KE, Pinkerton RM. The characteristics of 78 related airfoil sections from tests in the variable-density wind tunnel. 1933;.

32. Barton DAW. A real-time controller (RTC) based on the Beaglebone Black; 20018 (accessed Sep, 2018). Available from: https://github.com/dawbarton/rtc.
33. Bohlin TP. Practical grey-box process identification: theory and applications. Springer Science & Business Media; 2006.
34. Abdelkefi A, Vasconcellos R, Nayfeh AH, Hajj MR. An analytical and experimental investigation into limit-cycle oscillations of an aeroelastic system. Nonlinear Dynamics. 2013;71(1-2):159–173.
35. Strganac TW, Ko J, Thompson DE. Identification and control of limit cycle oscillations in aeroelastic systems. Journal of Guidance, Control, and Dynamics. 2000;23(6):1127–1133.
36. Ruzzene M, Fasana A, Garibaldi L, Piombo B. Natural frequencies and dampings identification using wavelet transform: application to real data. Mechanical systems and signal processing. 1997;11(2):207–218.
37. Pintelon R, Schoukens J. System identification: a frequency domain approach. John Wiley & Sons; 2012.
38. Ljung L. System identification. Wiley Encyclopedia of Electrical and Electronics Engineering. 2001;.
39. Char BW, Fee GJ, Geddes KO, Gonnet GH, Monagan MB. A tutorial introduction to Maple. Journal of Symbolic Computation. 1986;2(2):179–200.